Inorganic Chemistry
Article

*Inorg. Chem.* **2010**, *49*, 5679–5685 **5679**
DOI: 10.1021/ic100699u

# Enhancement of the Curie Temperature along the Perovskite Series $RCu_3Mn_4O_{12}$ Driven by Chemical Pressure of $R^{3+}$ Cations (R = Rare Earths)

**Javier Sánchez-Benítez,[†] José Antonio Alonso,*[,†] María Jesús Martínez-Lope,[†] Alicia de Andrés,[†] and María Teresa Fernández-Díaz[‡]**

[†]*Instituto de Ciencia de Materiales de Madrid, CSIC, Cantoblanco, E-28049 Madrid, Spain, and*
[‡]*Institut Laue-Langevin, BP156X, Grenoble, F-38042, France*

Received April 12, 2010

The compounds of the title series have been prepared from citrate precursors under moderate pressure conditions ($P$ = 2 GPa) and 1000 °C in the presence of $KClO_4$ as oxidizing agent. The crystal structures are cubic, space group $Im\bar{3}$ (No. 204); the unit cell parameters linearly vary from $a$ = 7.3272(4) Å (R = La) to $a$ = 7.2409(1) Å (R = Lu) at room temperature. A neutron or synchrotron X-ray diffraction study of all the members of the series reveals an interesting correlation between some structural parameters and the magnetic properties. The electron injection effect upon replacement of $Ca^{2+}$ with $R^{3+}$ cations in the parent $CaCu_3Mn_4O_{12}$ oxide leads to a substantial increment of the ferrimagnetic Curie temperature ($T_C$). An essential ingredient is supplied by the internal pressure of the $R^{3+}$ cations upon a decrease in size along the rare-earth series, from La to Lu: the concomitant compression of the $MnO_6$ octahedral units for the small rare earths provides progressively shorter Mn−O distances and improves the overlapping between Mn and O orbitals, thereby promoting superexchange and enhancing $T_C$ by 50 K along the series. This interaction is also reinforced by a ferromagnetic component that depends on the local distortion of the $MnO_6$ octahedra, which also increases along the series, constituting an additional factor, via intersite virtual charge transfer t−e orbital hybridization, for the observed increment of $T_C$.

## Introduction

There are very few half-metallic ferromagnetic oxides that can be used as magnetoresistive materials, the electrical conductivity of which changes upon application of an external magnetic field.[1] Besides the most extensively studied hole-doped manganese perovskites[2,3] and other selected oxides such as the double perovskite $Sr_2FeMoO_6$[4,5] and the pyrochlore $Tl_2Mn_2O_7$ and derivatives,[6−9] the choice has been expanded upon the description of a good low-field magnetoresistive response for the complex perovskite $CaCu_3Mn_4O_{12}$,[10−13] exhibiting the required stability around room temperature for technical applications. This oxide is, in fact, a spin-asymmetric ferrimagnetic ($T_C$ = 355 K) semiconductor, where Cu spins are antiferromagnetically coupled to Mn magnetic moments and the existence of a spin-dependent gap implies a thermally induced transport that is 100% polarized.[12]

The crystal structure of $CaCu_3Mn_4O_{12}$ is a 4-fold superstructure of perovskite $ABO_3$, driven by the long-range ordering of Ca and Cu at the A positions of the perovskite, in a $2a_0 \times 2a_0 \times 2a_0$ cubic cell of $Im\bar{3}$ symmetry ($a_0$: unit cell of the perovskite aristotype).[14−17] Given the small size of $Ca^{2+}$ and $Cu^{2+}$ cations, the $MnO_6$ octahedra are strongly tilted

*To whom correspondence should be addressed. E-mail: ja.alonso@icmm.csic.es.

(1) Ramirez, A. P. *J. Phys.: Condens. Matter* **1997**, *9*, 8171–8199.
(2) von Helmholt, R.; Wecker, J.; Holzapfel, B.; Schultz, L.; Samwer, K. *Phys. Rev. Lett.* **1993**, *71*, 2331–2333.
(3) Jin, S.; Tiefel, T. H.; McCormack, M.; Fastnach, R. A.; Ramesh, R.; Chen, L. H. *Science* **1994**, *246*, 413–415.
(4) Kobayashi, K.-I.; Kimura, T.; Sawada, H.; Terakura, K.; Tokura, Y. *Nature* **1998**, *395*, 677–680.
(5) Retuerto, M.; Alonso, J. A.; Martínez-Lope, M. J.; Martínez, J. L.; García-Hernández, M. *Appl. Phys. Lett.* **2004**, *85*, 266–268.
(6) Shimakawa, Y.; Kubo, Y.; Manako, T. *Nature* **1996**, *379*, 53–55.
(7) Subramanian, M. A.; Toby, B. H.; Ramirez, A. P.; Marshall, W. J.; Sleight, A. W.; Kwei, G. H. *Science* **1996**, *273*, 81–84.
(8) Alonso, J. A.; Martínez, J. L.; Martínez-Lope, M. J.; Casais, M. T.; Fernández-Díaz, M. T. *Phys. Rev. Lett.* **1999**, *82*, 189–192.
(9) Alonso, J. A.; Velasco, P.; Martínez-Lope, M. J.; Casais, M. T.; Martínez, J. L.; Fernández-Díaz, M. T.; de Paoli, J. M. *Appl. Phys. Lett.* **2000**, *76*, 3274–3276.
(10) Zeng, Z.; Greenblatt, M.; Subramanian, M. A.; Croft, M. *Phys. Rev. Lett.* **1999**, *82*, 3164–3167.
(11) Wu, H.; Zheng, Q.; Gong, X. *Phys. Rev. B* **2000**, *61*, 5217–5222.
(12) Weht, R.; Pickett, W. E. *Phys. Rev. B* **2001**, *65*, 14415–14421.
(13) Troyanchuk, I. O.; Lobanovsky, L. S.; Kasper, N. V.; Hervieu, M.; Maignan, A.; Michel, C.; Szymczak, H.; Szewczyk, A. *Phys. Rev. B* **1998**, *58*, 14903–14907.
(14) Deschanvres, A.; Raveau, B.; Tollemer, F. *Bull. Soc. Chim. Fr.* **1967**, 4077–4078.
(15) Chenavas, J.; Joubert, J. C.; Marezio, M.; Bochu, B. *J. Solid State Chem.* **1975**, *14*, 25–32.
(16) Bochu, B.; Chenavas, J.; Joubert, J. C.; Marezio, M. *J. Solid State Chem.* **1974**, *11*, 88–93.
(17) Marezio, M.; Dernier, P. D.; Chenavas, J.; Joubert, J. C. *J. Solid State Chem.* **1973**, *6*, 16–20.


Published on Web 05/12/2010

(showing Mn−O−Mn angles of ∼141°), thus conforming a highly irregular oxygen coordination environment around $Cu^{2+}$, almost in a square-planar configuration, as required for this Jahn−Teller cation. The synthesis of this material, and that of other compounds of the $A'A_3B_4O_{12}$ family, has been described to require high-pressure conditions (7 GPa), necessary to stabilize the small A cations in the 12-fold positions of the perovskite. Recently, we have been able to synthesize some new derivatives of $CaCu_3Mn_4O_{12}$ at moderate pressures of 2 GPa, starting with very reactive precursors, obtained by wet-chemistry techniques.[18]

$Ca^{2+}$ cations can be replaced by rare earths in the $RCu_3Mn_4O_{12}$ (R = rare earths) family. These compounds must also be prepared under high-pressure conditions. In their pioneering work, Bochu et al.[19] first prepared the $RCu_3Mn_4O_{12}$ oxides by hydrothermal synthesis, finding that a large amount of $Mn^{3+}$ is located at $Cu^{2+}$ sites; they found $T_C$'s ranging between 400 (R = Y) and 430 K (R = Th), although a trend along the series was not described. For some members of this series (R = La, Pr, Tb, Dy, Ho, Tm, and Yb) prepared at 2 GPa, we subsequently found that the concomitant electron-doping effect dramatically affects the magnetic and transport properties.[20−22] In the present work we have synthesized, also at 2 GPa in a piston-cylinder press, some new members of the family, for R = Nd, Sm, Eu, Gd, Y, Er, and Lu, for which we describe magnetization and magnetotransport data. The materials with nonabsorbing rare earths have been studied by neutron powder diffraction, whereas the absorbing materials for R = Sm, Eu, and Gd were studied by synchrotron X-ray diffraction, allowing us to determine the subtle structural features that are related to the observed physical properties. In fact, the ferromagnetic $T_C$ increases remarkably along the series, exceeding 400 K. A metallic behavior in the entire temperature range is observed, due to the electron injection effect. A global inspection of the full series, from La to Lu, allowed us to unveil a remarkable correlation between some features of the crystal structure and the magnetism of these oxides.

## Experimental Section

The elaboration of these materials required the previous preparation of reactive precursor powders by a wet-chemistry technique. Stoichiometric amounts of analytical grade $R_2O_3$ (R = Nd, Sm, Eu, Gd, Y, Er, Lu), $Cu(NO_3)_2 \cdot 3H_2O$, and $MnCO_3$ were dissolved in citric acid. The solution was slowly evaporated, leading to an organic resin, which was dried at 120 °C. The sample was then heated at 600 °C for 12 h in order to eliminate all the organic materials and nitrates. The so-formed precursor powders were thoroughly ground with $KClO_4$ and put into a gold capsule (8 mm diameter, 10 mm length), sealed, and placed in a cylindrical graphite heater. The reaction was carried out in a piston-cylinder press (Rockland Research Co.), at a hydrostatic pressure of 2 GPa at 1000 °C for 60 min. Then the materials were quenched to room temperature, and the pressure was subsequently released. The in-situ decomposition of $KClO_4$ provides the high $O_2$ pressure required to stabilize $Mn^{4+}$ cations. A fraction of the raw products, obtained as dense, homogeneous pellets, was partially ground to perform the structural and magnetic characterization; some as-grown pellets were kept for magnetotransport measurements. The ground product was washed in a dilute $HNO_3$ aqueous solution, in order to dissolve KCl coming from the decomposition of $KClO_4$ and to eliminate small amounts of unreacted CuO; then the powder samples were dried in air at 150 °C for 1 h.

The characterization by XRD was performed using a Bruker-AXS D8 diffractometer (40 kV, 30 mA), controlled by DIFFRACT$^{plus}$ software, in Bragg−Brentano reflection geometry with Cu K$\alpha$ radiation ($\lambda$ = 1.5418 Å). A secondary graphite monochromator allowed the complete removal of Cu K$\beta$ radiation. The data were obtained between 10° and 100° 2$\theta$ in steps of 0.05°. Room-temperature high-resolution NPD patterns of $RCu_3Mn_4O_{12}$ (R = Nd, Y, Er, and Lu) were collected at the D2B diffractometer of the Institut Laue-Langevin, Grenoble, with a wavelength $\lambda$ = 1.594 Å. The samples, weighing around 0.8 g, were contained in a vanadium holder, and a counting time of 4 h was required in the high-flux mode for each pattern. For R = Sm, Eu, and Gd high-resolution synchrotron X-ray diffraction patterns were collected at the SpLine beamline at ESRF (Grenoble), with $\lambda$ = 0.8255 Å. The samples were contained in a borosilicate-glass capillary; the data were collected at room temperature between 6° and 60° 2$\theta$ in steps of 0.01° with a counting time of 5 s per step. The NPD and XRD patterns were analyzed by the Rietveld method, using the FULLPROF program.[23] The line shape of the diffraction peaks was generated by a pseudo-Voigt function, and the background refined to a fifth-degree polynomial. No regions were excluded in the refinement. In the final run the following parameters were refined: background coefficients, zero-point, half-width, pseudo-Voigt, and asymmetry parameters for the peak shape; scale, positional, and occupancy factors for oxygens, thermal isotropic factors for all the atoms, and unit-cell parameters.

The dc magnetic susceptibility was measured with a commercial SQUID magnetometer on powdered samples in the temperature range 5−650 K with an applied field of 0.1 T; magnetization isotherms were recorded between −5 and +5 T. Transport and magnetotransport measurements were performed by the conventional four-probe technique, under magnetic fields up to 9 T in a PPMS system from Quantum Design.

## Results

**Crystal Structure.** The reaction products were identified as single-phase cubic perovskites by XRD. A representative XRD diagram corresponding to $LuCu_3Mn_4O_{12}$ is illustrated in Figure SI-1 (Supporting Information). The pattern shows sharp, well-defined superstructure reflections due to the 1:3 ordering of R and Cu cations. No impurity phases were detected from either XRD or NPD data. Identical diagrams were obtained for all the samples. A neutron powder diffraction (NPD) (R = Nd, Y, Er, and Lu) or synchrotron XRD (R = Sm, Eu, and Gd) study was essential to investigate the structural details of the R-substituted samples.

The NPD and synchrotron XRD patterns were refined by the Rietveld method taking as starting model that described for $CaCu_3Mn_4O_{12}$, space group $Im\bar{3}$, $Z$ = 2.

(18) Sánchez-Benítez, J.; Alonso, J. A.; Martínez-Lope, M. J.; Casais, M. T.; Martínez, J. L.; de Andrés, A.; Fernández-Díaz, M. T. *Chem. Mater.* **2003**, *15*, 2193–2200.
(19) Bochu, B.; Joubert, J. C.; Collomb, A.; Ferrand, B.; Samaras, D. *J. Magn. Magn. Mater.* **1980**, *15−18*, 1319–1321.
(20) Alonso, J. A.; Sánchez-Benítez, J.; de Andrés, A.; Martínez-Lope, M. J.; Casais, M. T.; Martínez, J. L. *Appl. Phys. Lett.* **2003**, *83*, 2623–2625.
(21) Sánchez-Benítez, J.; Alonso, J. A.; de Andrés, A.; Martínez-Lope, M. J.; Martínez, J. L.; Muñoz, A. *Chem. Mater.* **2005**, *17*, 5070–5076.
(22) Sánchez-Benítez, J.; Alonso, J. A.; Falcón, H.; Martínez-Lope, M. J.; de Andrés, A.; Fernández-Díaz, M. T. *J. Phys.: Condens. Matter* **2005**, *17*, S3063–S3068.
(23) Rodríguez-Carvajal, J. *Phys. B* (*Amsterdam, Neth.*) **1993**, *192*, 55–69.

**Table 1.** Unit-Cell, Positional, and Thermal Parameters and Ordered Magnetic Moments (and Reliability Factors) for $RCu_3Mn_4O_{12}$ in the Cubic $Im\bar{3}$ (No. 204) Space Group, $Z = 2$, from NPD Data and Synchrotron XRD Data at 295 K

| | | Nd | Sm | Eu | Gd | Y | Er | Lu |
|---|---|---|---|---|---|---|---|---|
| $a$ (Å) | | 7.2930(3) | 7.28483(2) | 7.2803(1) | 7.2744(1) | 7.25600(8) | 7.25188(9) | 7.2409(1) |
| $V$ (Å$^3$) | | 387.90(3) | 386.60(2) | 385.879(9) | 384.94(1) | 382.023(7) | 381.375(8) | 379.641(9) |
| R | 2*a* (0 0 0) | | | | | | | |
| $B$ (Å$^2$) | | 0.70(12) | 0.28(3) | 0.45(2) | 0.71(4) | 0.66(6) | 0.59(6) | 0.08(4) |
| (Cu,Mn2) | 6*b* (0 1/2 1/2) | | | | | | | |
| $B$ (Å$^2$) | | 0.84(9) | 0.61(4) | 0.65(4) | 0.85(5) | 0.49(3) | 0.52(4) | 0.26(2) |
| $f_{occ}$(Cu) | | 0.928(7) | 1.0(1) | 0.99(7) | 0.98(7) | 0.973(6) | 0.984(6) | 0.992(6) |
| magn. mom. ($\mu_B$) | | −0.8(4) | | | | −0.5(3) | −0.8(3) | −0.6(4) |
| Mn1 | 8*c* (1/4 1/4 1/4) | | | | | | | |
| $B$ (Å$^2$) | | 1.09(7) | 0.34(3) | 0.47(3) | 0.65(4) | 0.55(3) | 0.63(4) | 0.25(2) |
| magn. mom. ($\mu_B$) | | 1.3(2) | | | | 1.67(5) | 1.73(5) | 1.18(11) |
| O | 24*g* (0 *y z*) | | | | | | | |
| $y$ | | 0.3019(7) | 0.3032(8) | 0.3023(7) | 0.3013(6) | 0.29864(14) | 0.29877(16) | 0.29727(18) |
| $z$ | | 0.1807(7) | 0.1818(9) | 0.1817(7) | 0.1806(6) | 0.17874(14) | 0.17928(15) | 0.17655(18) |
| $B$ (Å$^2$) | | 1.09(4) | 0.97(12) | 1.28(11) | 0.50(12) | 0.52(2) | 0.58(2) | 0.25(1) |
| reliability factors | | | | | | | | |
| $\chi^2$ | | 1.24 | 37.2 | 25.9 | 16.5 | 1.10 | 0.78 | 1.23 |
| $R_p$ (%) | | 7.90 | 8.95 | 7.78 | 4.59 | 3.57 | 3.14 | 1.61 |
| $R_{wp}$ (%) | | 9.91 | 12.1 | 10.0 | 6.40 | 4.68 | 4.06 | 2.04 |
| $R_I$ (%) | | 9.77 | 7.66 | 7.73 | 2.50 | 4.56 | 4.12 | 1.50 |
| $R_{mag}$ (%) | | 8.80 | | | | 6.57 | 7.05 | 10.8 |

R atoms were placed at 2*a* (0,0,0) positions, Cu at 6*b* (0, 1/2,1/2) positions, Mn at 8*c* (1/4,1/4,1/4), and O at 24*g* (*x*,*y*,0) sites. Reasonable fits were obtained for this preliminary model. As a second step, Mn atoms were introduced at random at 6*b* positions together with Cu, and the complementary occupancy factors were refined, constrained to a full occupancy. For R = Nd a significant amount [7.2(7)%] of Cu was found to be replaced by Mn; for the remaining rare earths the Mn content at 6*b* site is considerably smaller (Table 1). The subsequent refinement of the occupancy factor for the oxygen positions gave no significant deviation from the full stoichiometry. Taking into account the amount of $Mn^{3+}$ localized at $Cu^{2+}$ positions (Table 1), the valence of Mn at the octahedral sites spans between 3.67+ for R = Nd and 3.75+ for R = Sm, Eu, and Lu. As the materials are ferrimagnetically ordered at room temperature (RT), the magnetic structure was included as a second phase in the final refinement for R = Nd, Y, Er, and Lu (NPD data); we have modeled a perfect ferrimagnetic ordering between the magnetic moments at 6*b* and 8*c* positions, directed along the *c* axis; this model corresponds to a perfect collinear arrangement of Cu and Mn spins. The ordered magnetic moments at RT are also listed in Table 1, as well as the relevant parameters after the refinement from NPD and synchrotron XRD data. The quality of the fits is displayed in Figures SI-2 and SI-3 (Supporting Information) for neutron and synchrotron X-ray diffraction patterns, respectively. Table SI-1 (Supporting Information) contains the main bond distances and angles.

**Magnetic Measurements.** The dc magnetic susceptibility versus temperature data for $RCu_3Mn_4O_{12}$ exhibit the abrupt increase characteristic of a spontaneous ferro- or ferrimagnetic ordering, as shown in Figure 1a. The magnetic data for $CaCu_3Mn_4O_{12}$[10] are also included for the sake of comparison. The inflection points in the susceptibility indicate the ferromagnetic Curie temperatures ($T_C$), which increase remarkably for the different rare-earth-substituted materials up to more than 400 K (see Table SI-2 in the Supporting Information). As indicated above, the study of the magnetic structures demonstrates that Mn and Cu spins are coupled antiferromagnetically. At low temperatures (< 100 K), the rare-earth moment plays an important role in the total magnetization for the strongly paramagnetic rare earths, i.e., in the Er and Gd perovskites. The rare-earth moment seems to become antiferromagnetically coupled with the Mn sublattice, and therefore the magnetization undergoes an important decrease (Figure 1a). The magnetization versus magnetic field plots are shown in Figure 1b. The saturation magnetization is reached for $H < 1$ T, showing a behavior characteristic of pure ferromagnets. For $ErCu_3Mn_4O_{12}$ (inset of Figure 1b) we observe that the magnetization data at 5 K reach smaller values than at 70 K. This is in good agreement with the susceptibility curve in Figure 1a, where a progressive decrease is observed below 70 K. The 5 K isotherm shows a progressive increment of the magnetization upon the external magnetic field; this can be explained as a progressive turning over of the Er magnetic moments from the orientation adopted in the magnetic structure stable at $H = 0$, where the Er moments are expected to be antiferromagnetically coupled to the Mn moments.

For R = Er the susceptibility was measured up to 650 K. Above $T_C$, the reciprocal susceptibility data (inset of Figure 1a) show a progressive change of slope, which diminishes as temperature increases. This behavior of the reciprocal susceptibility is a typical feature of ferrimagnetic compounds. The data nicely fit the formula $\chi^{-1} = \frac{T^2 - \theta^2}{(C_A + C_B)T - 2\lambda C_A C_B}$, which represents the reciprocal susceptibility of the paramagnetic phase of a ferrimagnetic compound,[24] where A and B stand for the two sublattices that experience antiferromagnetic coupling below the ordering temperature. The fit to the total paramagnetic range (400−650 K) gives the $C_A = 12.2$ and $C_B = 8.9$ Curie constants, from which we obtain the effective paramagnetic moments of 9.92 $\mu_B$/f.u. and 8.5 $\mu_B$/f.u. for both A

(24) Kittel, C. *Introduction to Solid State Physics*; John Wiley: New York, 1993.

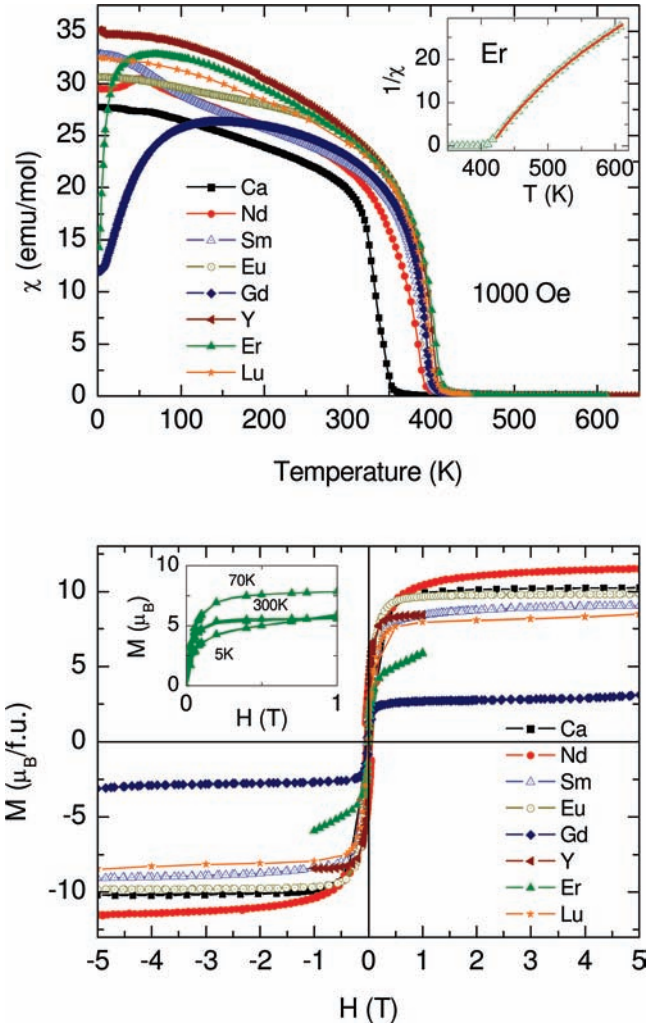


**Figure 1.** (a) Temperature dependence of the dc magnetic susceptibility for the $RCu_3Mn_4O_{12}$ series. Inset shows the Er reciprocal susceptibility curve fit. (b) Magnetization versus magnetic field isotherms at 5 K. The inset illustrates the isotherms at different temperatures for the Er sample.

$(Cu^{2+}/Er^{3+})$ and B $(Mn^{3+/4+})$ sublattices, very close to the expected of 10.0 $\mu_B$/f.u. and 8.3 $\mu_B$/f.u. obtained considering the standard values of $\mu_{para}$ = 9.5, 1.73, 4.9, and 3.87 $\mu_B$ for $Er^{3+}$, $Cu^{2+}$, $Mn^{3+}$, and $Mn^{4+}$, respectively. The obtained Weiss constant, $\theta$ = 407 K, is significantly close to the Curie temperature and indicates the predominance of ferromagnetic interactions in the system.

**Magnetotransport Measurements.** Figure 2 displays the transport properties of $RCu_3Mn_4O_{12}$ (R = Nd, Eu, Gd, Er). The resistivity at $H$ = 0 displays a metallic behavior in the temperature range $2 < T < 400$ K, except for Gd, which shows a metal−insulator transition at around 260 K. It is worth mentioning that the observed value for $\rho(T = 300\text{K}, H = 0) = 6.3 \times 10^{-4}$ Ω·cm for Er is considerably smaller than that of the other members of the series, which can be correlated with the structural features. The metallic behavior and the low resistivity can be explained by the partial filling of the $e_g$ Mn band of the Mn located at the B site.[25] The magnetoresistance of these compounds can be defined as

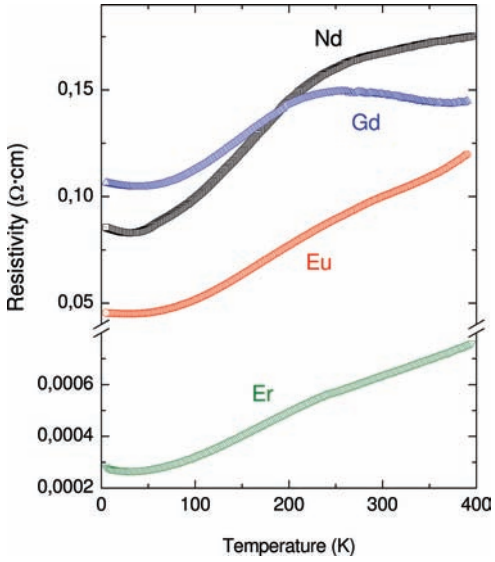


**Figure 2.** Resistivity versus temperature plot for $RCu_3Mn_4O_{12}$ (R = Nd, Eu, Gd, Er).

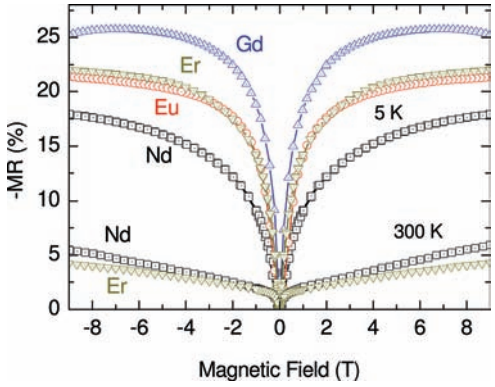


**Figure 3.** Magnetoresistance isotherms at 5 and 300 K for R = Nd, Eu, Gd, Er. MR is defined as $100 \times [R(H) - R(0)]/R(0)$.

$MR(H) = 100 \times [R(H) - R(0)]/R(0)$. Figure 3 illustrates some selected isotherms for external applied fields $-9 < H < 9$ T. A maximum negative MR of 20−25% is achieved at 5 K for $H$ = 9 T; MR is still significant at RT for R = Nd and Er, displaying values close to −5% for $H$ = 9 T.

## Discussion

The cubic, body-centered crystal structure of the $RCu_3Mn_4O_{12}$ perovskites is represented in Figure 4, showing as a main feature the significant tilting of the $MnO_6$ octahedra, which is a consequence of the small size of $R^{3+}$ and $Cu^{2+}$ cations occupying the A positions. The variation of the $a$ unit-cell parameter versus the $R^{3+}$ ionic radius[26] is displayed in Figure 5, including the remaining members of the series for $R^{3+}$ rare-earth cations[21,22] as well as $Ce^{4+}$,[27] $Th^{4+}$,[28] and $Ca^{2+}$,[15] as a reference. There is a considerable increment of this parameter with respect to that reported for $CaCu_3Mn_4O_{12}$: from the chemical point of view, the presence of

(25) Sánchez-Benítez, J.; Prieto, C.; de Andrés, A.; Alonso, J. A.; Martínez-Lope, M. J.; Casais, M. T. *Phys. Rev. B* **2004**, *70*, 24419.

(26) Shannon, R. D. *Acta Crystallogr.* **1976**, *A 32*, 751–767.

(27) Sánchez-Benítez, J.; Martínez-Lope, M. J.; Alonso, J. A. *J. Appl. Phys.* **2010**, doi: 10.1063/1.3369444.

(28) Sánchez-Benítez, J.; Martínez-Lope, M. J.; Alonso, J. A. *Z. Naturforsch.* **2008**, *63b*, 1–6.

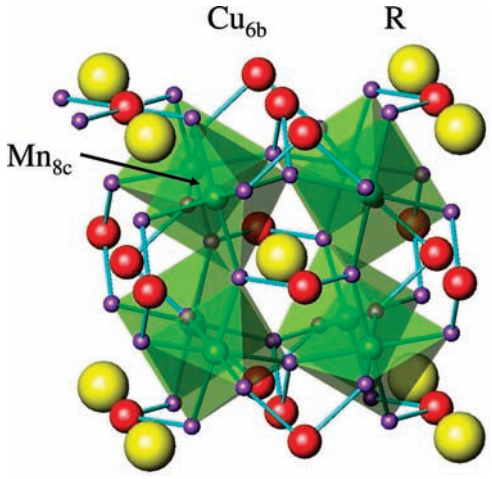


**Figure 4.** View of the crystal structure of $RCu_3Mn_4O_{12}$. Corner-sharing $MnO_6$ octahedra are fairly tilted in the structure to optimize R−O and Cu−O bond lengths; Cu atoms are bonded to four oxygens in a pseudo-square-planar coordination.

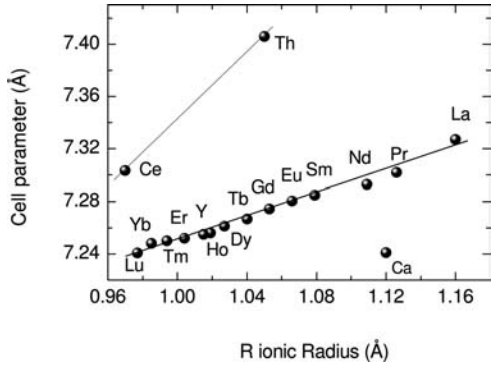


**Figure 5.** Evolution of the *a* unit-cell parameter for the full $RCu_3Mn_4O_{12}$ series with the ionic radius of *R*. The parameter for $CaCu_3Mn_4O_{12}$ is given as a reference.[15] The lines are guides to the eye.

$R^{3+}$ cations replacing $Ca^{2+}$ in $CaCu_3Mn_4O_{12}$ implies the reduction of one $Mn^{4+}$ cation to $Mn^{3+}$, giving rise to an average nominal valence for Mn of 3.75+, as mentioned above. The possible presence of some oxygen vacancies per formula unit was discarded by the neutron powder diffraction study for Nd, Y, Er, and Lu. In the case of $Ce^{4+}$ and $Th^{4+}$ this electron injection effect is double, which is evident in an additional expansion of the unit cell, as shown in Figure 5.

At the B substructure of the perovskite, ($Mn^{4+}$, $Mn^{3+}$) cations occupy the center of axially distorted octahedra with six equal Mn−O distances. Figure 6a shows the evolution of the Mn−O distances (taken from Table SI-1) completed with those corresponding to the remaining rare-earth compounds,[21,22] Ce,[27] Th,[28] and Ca.[15] The Mn−O distances progressively increase along the $R^{3+}$ series, as shown in the figure. Due to the incorporation of larger $Mn^{3+}$ cations in the $Mn^{4+}$ sublattice, the Mn−O bonds are significantly expanded with respect to the parent $CaCu_3Mn_4O_{12}$ perovskite (Mn−O: 1.915(1) Å[15]), as also illustrated in Figure 6a. R atoms are coordinated to 12 oxygen atoms, with equal R−O distances. Also, the R−O bond lengths (Figure 6b) linearly correlate with the size of the rare-earth cation. On the other hand the oxygen environment for $Cu^{2+}$ cations is highly irregular, with eight rather long distances (Table SI-1) and an effective

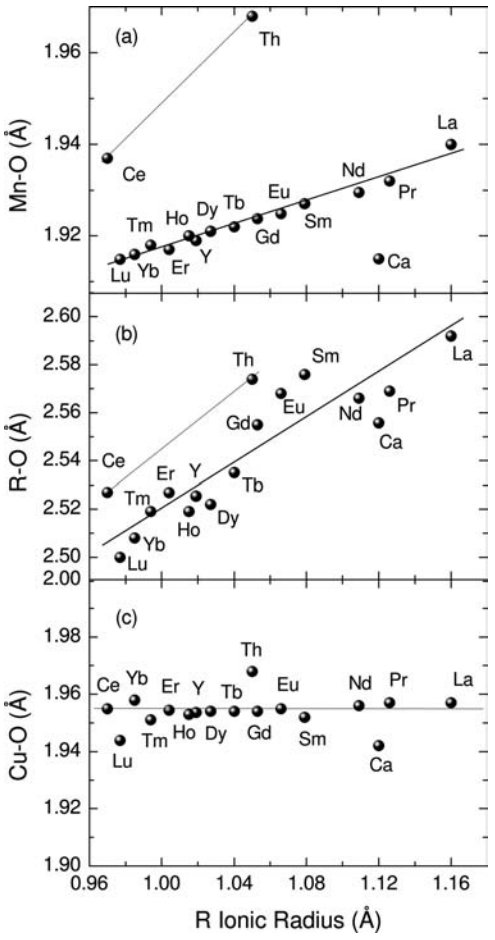


**Figure 6.** Variation of (a) Mn−O distances, (b) R−O distances, and (c) Cu−O distances along the $RCu_3Mn_4O_{12}$ series. The lines are guides to the eye.

coordination number of four, in a pseudosquare arrangement. The Cu−O distances, represented in Figure 6c as a function of the $R^{3+}$ ionic radius, are virtually unchanged along the series.

It is interesting to notice that the tilting angle of the $MnO_6$ octahedra, quantified from the Mn−O−Mn angle, does not significantly vary across the series, as illustrated in Figure 7. This fact is in sharp contrast with the observed behavior in most of the series of rare-earth perovskites of general formula $RMO_3$ (M = transition metals) where the reduction in the tolerance factor induced by the contraction of the $R^{3+}$ ionic radius along the series (from La to Lu) is accommodated in the perovskite structure by a concomitant increase in the tilting angle of the $MO_6$ octahedra, in order to optimize the R−O distances.[29−31] In the present case, the tilting of the $MnO_6$ octahedra is mainly determined by the presence of three $Cu^{2+}$ versus a single $R^{3+}$ cation at the A′ positions; therefore the Cu−O square-planar units strongly "lock" the Mn−O−Mn angles of the full series. We will come back to this point later on, as this fact will have serious implications on the evolution of the magnetic behavior along the series.

(29) Olés, A.; Kajzar, F.; Kucab, M.; Sikora, W. *Magnetic Structures Determined by Neutron Diffraction*; Naukowe, P. W., Ed.; Krakov, Warsaw, 1976.
(30) García-Muñoz, J. L.; Rodríguez-Carvajal, J.; Lacorre, P.; Torrance, J. B. *Phys. Rev. B* **1992**, *46*, 4414–4425.
(31) Marezio, M.; Remeika, J. P.; Dernier, P. D. *Acta Crystallogr.* **1970**, *B26*, 2008–2022.

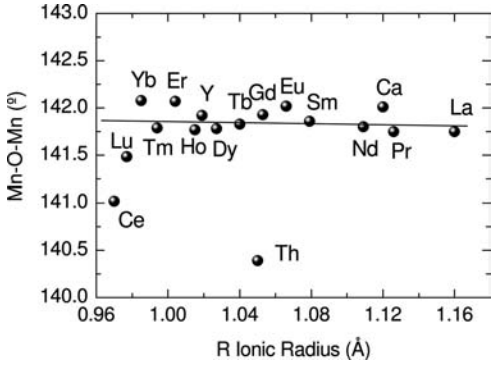


**Figure 7.** Mn−O−Mn angle, indicating the tilting of the $MnO_6$ octahedra, versus the *R* ionic radius. The line is a guide to the eye.

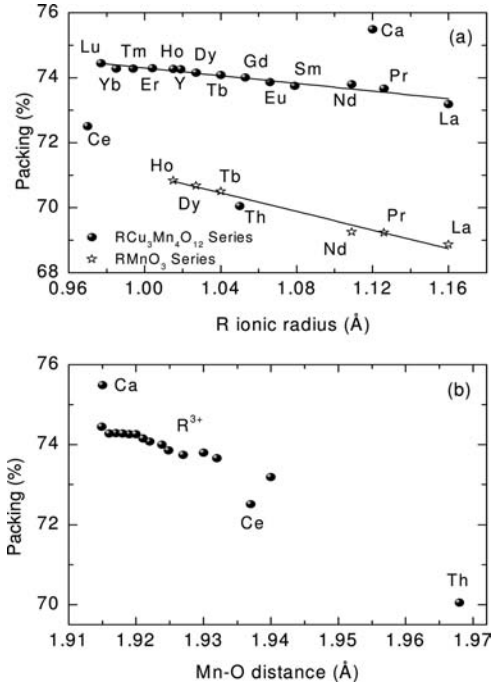


**Figure 8.** (a) Variation of the packing index of the $RCu_3Mn_4O_{12}$ series with the R ionic radius. Values for the $RMnO_3$ series are given for the sake of comparison calculated from ref 31. (b) Evolution of the compactness of the structure along the series versus Mn−O bond lengths. The lines are guides to the eye.

An interesting aspect that is worth examining is the "packing index" in these oxides. This parameter can be defined as the ratio of the sums of the atom volumes over the unit-cell volume. The packing index gives an idea of the space actually occupied by the atoms in a certain crystal structure and thus describes the compactness of this structure. Figure 8a represents the packing index of the $RCu_3Mn_4O_{12}$ oxides versus the ionic radii of the rare earths, observing a linear relationship for the trivalent $R^{3+}$ cations. This indicates that the structure tends to be less compact when the ionic radius increases, which is to say that the unit-cell volume increases faster than the ionic radius. Notice that the divalent and tetravalent cations are clearly outside this trend. However, if we represent the variation of the packing index versus the Mn−O distance (Figure 8b), we observe that the packing factor reasonably scales with the Mn−O bond lengths, including the Ca, Ce, and Th compounds: the compactness of the structure is governed by the Mn−O bond

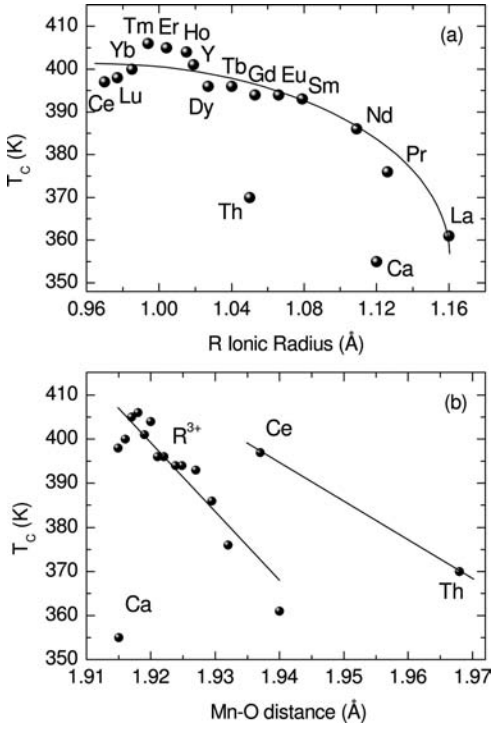


**Figure 9.** Evolution of the Curie temperature, $T_C$, along the $RCu_3Mn_4O_{12}$ series with the (a) ionic radius and (b) the Mn−O distance. The lines are guides to the eye.

lengths; thus the structure is less packed for large Mn−O distances. It is also interesting to compare the $RCu_3Mn_4O_{12}$ oxides with the series of simple perovskites $RMnO_3$.[32] In $RMnO_3$ the B position is occupied only by $Mn^{3+}$, in such a way that the average Mn−O distance is longer than in the $RCu_3Mn_4O_{12}$ series. In Figure 8a we observe that the simple $RMnO_3$ perovskites present a significantly lower packing index than the complex perovskites. The main difference is that 75% of the A sites in $RCu_3Mn_4O_{12}$ are occupied by $Cu^{2+}$ ions, which are able to form strongly covalent bonds to oxygen atoms; this fact accounts for the higher compactness of the structure. In conclusion, the degree of packing of these systems mainly depends on the degree of covalence of the chemical bonds: both $Mn^{4+}$−O and $Cu^{2+}$−O are fairly covalent, accounting for a higher degree of global covalence for $RCu_3Mn_4O_{12}$.

The dc magnetic susceptibility versus temperature data for $RCu_3Mn_4O_{12}$ exhibit a spontaneous ferromagnetic ordering for all the samples, with $T_C$ increasing remarkably up to more than 400 K, well above the reported Curie temperature of the parent compound $CaCu_3Mn_4O_{12}$ ($T_C$ = 355 K).[10] The evolution of $T_C$ along the series of rare-earth cations is shown in Figure 9a. There is an overall increase of the Curie temperature as the rare-earth size diminishes, from La to Lu. Again, this is in sharp contrast with that observed in many series of magnetic $RMO_3$ perovskites, where a reduction in the size of $R^{3+}$ is usually accompanied with a decrease of the long-range ordering temperature (ferromagnetic $T_C$ or antiferromagnetic $T_N$), as illustrated for the series of $RMnO_3$ antiferromagnetic perovskites, where $T_N$ varies from 130 K (R = La) to 41 K (R = Ho) (indeed there is a transition from

(32) Alonso, J. A.; Martínez-Lope, M. J.; Casais, M. T.; Fernández-Díaz, M. T. *Inorg. Chem.* **2000**, *39*, 917–923.

type-E to type-A ordering; $T_N$ for the phase of type E ordering does not depend on the R size) or for the $RFeO_3$ antiferromagnets, where $T_N$ evolves from 750 K (R = La) to 623 K (R = Lu). This is ascribed to the progressive increase of the tilting angle as $R^{3+}$ becomes smaller,[29−31] bending the superexchange Mn−O−Mn angle and impairing the overlapping between Mn 3d and O 2p orbitals, thus weakening the long-distance magnetic interactions.

The crystal structure of the complex perovskites $RCu_3Mn_4O_{12}$ is odd in the sense that a reduction in the size of the $R^{3+}$ cations along the rare-earth series from La to Lu is not accommodated by the perovskite through an increase of the rotation angle of the $MnO_6$ octahedra, since the tilting angle is mainly determined by the $CuO_4$ square-planar units placed at the A positions of the perovskite. Nevertheless, it is also observed that the cubic unit-cell parameter, *a*, progressively shrinks as $R^{3+}$ becomes smaller, scaling with the size of the rare-earth cation. Since the rotation angle of the $MnO_6$ octahedra is blocked by the $CuO_4$ units, the reduction in size of the $RO_{12}$ coordination polyhedra (Figure 6b) is accommodated by a concomitant shrinking of the $MnO_6$ octahedra along the series, leading to the observed reduction in Mn−O distances illustrated in Figure 6a. We believe that this gradual compression effect of the Mn−O bonds is one of the clues to understand the progressive increment of the Curie temperatures along the $RCu_3Mn_4O_{12}$ series. Figure 9b shows that there is a linear relationship between the observed $T_C$'s and the lengths of the Mn−O bonds, confirming the hypothesis that the magnetic interactions are mainly controlled by this distance. In fact, the internal pressure or chemical pressure produced by the diminution of $R^{3+}$ cations is responsible for the compression of the Mn−O chemical bonds, thus improving the overlapping between 3d Mn and 2p O orbitals and enhancing the superexchange mechanism and the strength of the magnetic interactions between Mn magnetic moments.

As a final consideration, the O−Mn−O angles that define the axial distortion of the $MnO_6$ octahedra also change with the $R^{3+}$ ionic size, as shown in Figure 10. We define this angular distortion as twice the deviation of the O−Mn−O angle with respect to 90°. The effect of the chemical pressure introduced as the $R^{3+}$ size diminishes not only compresses the Mn−O distances but also leads to a progressive angular distortion of the $MnO_6$ octahedra with respect to a ternary axis along the [1 1 1] direction. This angular distortion may also have an important influence on the magnetic coupling between adjacent Mn atoms, reinforcing the ferromagnetism. In compounds with $Mn^{4+}$, only containing half-filled t orbitals, it is important to take into account a spin−spin interaction term in addition to the superexchange interaction $J^{\pi}$, fully dependent on the Mn−O distances and Mn−O−Mn angles. It has been shown that the hybridization between t and e orbitals of adjacent sites is highly sensitive to the O−Mn−O angle,[33] a continuous reduction of which (i.e., an increment of the octahedral distortion as observed in Figure 10) leads to a progressive enhancement of the hybridization. In the case of $Mn^{4+}$ the t−e hybridization due to the local site distortion introduces a virtual charge transfer to an empty e orbital,

(33) Landron, S.; Lepetit, B.-M. *Phys. Rev. B* **2008**, *77*, 125106.

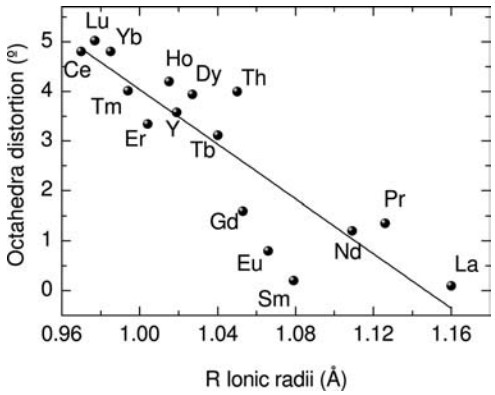


**Figure 10.** Axial distortion of the $MnO_6$ octahedra, defined as twice the deviation of the O−Mn−O angle with respect to 90°, versus the R ionic radius. The line is a guide to the eye.

which is ferromagnetic. The global FM superexchange interaction is thus reinforced as $J = J^{\pi} + J^{\sigma}_{hb}$ by a ferromagnetic component $J^{\sigma}_{hb}$ that depends on the local distortion, constituting an additional ingredient for the observed increment of $T_C$ as the rare-earth size decreases along the $R^{3+}$ series.

## Conclusions

We have demonstrated that the electron injection effect induced upon replacing Ca with rare earths in $CaCu_3Mn_4O_{12}$ gives rise to a substantial increment of the Curie temperature, probably ascribed to the presence of $Mn^{3+}$ at the octahedral positions of the perovskite, carrying a larger magnetic moment than $Mn^{4+}$. This electron injection effect is constant along the series (1 electron per formula). However we observe an additional enhancement of $T_C$ as the $R^{3+}$ size becomes smaller, which we ascribe to the internal pressure implemented by the small rare-earth cations on the Mn−O bonds and O−Mn−O angles. This overall scaling effect of the unit-cell size and the microscopic compression of the $MnO_6$ octahedra as $R^{3+}$ diminishes promotes the orbital overlap and enhances the long-range magnetic interactions; on the other hand, the local-site distortion enables a virtual t−e charge transfer that is ferromagnetic and increases along the series. The global FM superexchange interaction is thus reinforced. Unlike $CaCu_3Mn_4O_{12}$, which needs to be prepared at very high pressures of 7 GPa, $RCu_3Mn_4O_{12}$ can be easily obtained under moderate conditions (2 GPa) starting from very reactive precursors in the presence of an oxidizing agent. The easiness of their preparation, compared to the Ca parent compound, and the improvement achieved in the properties of interest, namely, the Curie temperature, make it possible to propose these magnetoresistant materials as candidates for practical applications in spintronic devices.

**Acknowledgment.** We thank CICyT for the financial support of the project MAT2007-60536, and we are grateful to ILL for making all facilities available and Prof. J. L. Martínez for the magnetic measurements.

**Supporting Information Available:** This material is available free of charge via the Internet at http://pubs.acs.org.